Simultaneous monitoring the real and imaginary parts of the analyte refractive index using liquid-core photonic bandgap Bragg fibers

Jingwen Li, Hang Qu, and Maksim Skorobogatiy*

École Polytechnique de Montréal, Montreal, Québec H3C3A7, Canada
**maksim.skorobogatiy@polymtl.ca*

Abstract: We demonstrate simultaneous monitoring of the real and imaginary parts of the liquid analyte refractive index by using a hollow-core Bragg fiber. We apply this two-channel fiber sensor to monitor concentrations of various commercial cooling oils. The sensor operates using spectral monitoring of the fiber bandgap center wavelength, as well as monitoring of the fiber transmission amplitude at mid-bandgap position. The sensitivity of the fiber sensor to changes in the real part of the core refractive index is found to be 1460nm/Refractive index unit (RIU). By using spectral modality and effective medium theory, we determine the concentrations of the two commercial fluids from the measured refractive indices with an accuracy of ~0.57% for both low- and high-loss oils. Moreover, using an amplitude-based detection modality allows determination of the oil concentration with accuracy of ~1.64% for low-loss oils and ~2.81% for the high-loss oils.

OCIS codes: (060.2310) Fiber optics; (060.2370) Fiber optics sensors; (060.5295) Photonic crystal fibers.

References and links

1. J. Beuthan, O. Minet, J. Helfmann, M. Herrig, and G. Müller, "The spatial variation of the refractive index in biological cells," Phys. Med. Biol. **41**(3), 369–382 (1996).
2. S. Singh, "Refractive index measurement and its applications," Phys. Scr. **65**(2), 167–180 (2002).
3. X. Fan, I. M. White, S. I. Shopova, H. Zhu, J. D. Suter, and Y. Sun, "Sensitive optical biosensors for unlabeled targets: A review," Anal. Chim. Acta **620**(1-2), 8–26 (2008).
4. B. Andreas Dahlin, *Plasmonic Biosensors- An Integrated View of Refractometric Detection* (IOS Press, 2012).
5. H. Yu, L. Xiong, Z. Chen, Q. Li, X. Yi, Y. Ding, F. Wang, H. Lv, and Y. Ding, "Solution concentration and refractive index sensing based on polymer microfiber knot resonator," Appl. Phys. Express **7**(2), 022501 (2014).
6. R. Manor, A. Datta, I. Ahmad, M. Holta, S. Gangopadhyay, and T. Dallsa, "Microfabrication and characterization of liquid core waveguide glass channels coated with Teflon AF," IEEE Sens. J. **3**(6), 687–692 (2003).
7. V. Benoit and M. C. Yappert, "Effect of capillary properties on the sensitivity enhancement in capillary/fiber optical sensors," Anal. Chem. **68**(1), 183–188 (1996).
8. Y. Han, M. K. Khaing, Y. Zhu, L. Xiao, M. S. Demohan, W. Jin, and H. Du, "Index-guiding liquid-core photonic crystal fiber for solution measurement using normal and surface-enhanced Raman scattering," Opt. Eng. **47**(4), 040502 (2008).
9. Y. Zhang, C. Shi, C. Gu, L. Seballos, and J. Zhang, "Liquid core photonic crystal fiber sensor based on surface enhanced Raman scattering," Appl. Phys. Lett. **90**(19), 193504 (2007).
10. H. F. Xuan, W. Jin, J. Ju, H. L. Ho, M. Zhang, and Y. B. Liao, "Low-contrast photonic bandgap fibers and their potential applications in liquid-base sensors," Proc. SPIE **6619**, 661936 (2007).
11. J. Sun and C. C. Chan, "Photonic bandgap fiber for refractive index measurement," Sens. Actuators B Chem. **128**(1), 46–50 (2007).
12. K. J. Rowland, S. Afshar, V. A. Stolyarov, Y. Fink, and T. M. Monro, "Spectral properties of liquid-core Bragg fibers," in: Conference on Lasers and Electro- Optics (CLEO), Baltimore, Maryland, US, June 2–4 2009.
13. H. Qu and M. Skorobogatiy, "Resonant bio- and chemical sensors using low-refractive-index-contrast liquid-core Bragg fibers," Sens. Actuators B Chem. **161**(1), 261–268 (2012).
14. H. Qu, B. Ung, M. Roze, and M. Skorobogatiy, "All photonic bandgap fiber spectroscopic system for detection of refractive index changes in aqueous analytes," Sens. Actuators B Chem. **161**(1), 235–243 (2012).

#237316 Received 23 Jun 2015; revised 17 Aug 2015; accepted 20 Aug 2015; published 24 Aug 2015

15. H. Qu and M. Skorobogatiy, "liquid-core low-refractive-index-contrast Bragg fiber sensor," Appl. Phys. Lett. **98**(20), 201114 (2011).
16. M. Skorobogatiy, "Efficient antiguiding of TE and TM polarizations in low-index core waveguides without the need for an omnidirectional reflector," Opt. Lett. **30**(22), 2991–2993 (2005).
17. M. Zourob and L. Akhlesh, *Optical Guided-Wave Chemical and Biosensors II* (Springer, 2010).
18. M. Skorobogatiy and J. Yang, *Fundamentals of Photonic Crystal Guiding* (Cambridge University Press, 2009).
19. W. M. Haynes, *CRC Handbook of Chemistry and Physics* (CRC Press, 2010).
20. G. A. Niklasson, C. G. Granqvist, and O. Hunderi, "Effective medium models for the optical properties of inhomogeneous materials," Appl. Opt. **20**(1), 26–30 (1981).
21. N. J. Hutchinson, T. Coquil, A. Navid, and L. Pilon, "Effective optical properties of highly ordered mesoporous thin films," Thin Solid Films **518**(8), 2141–2146 (2010).
22. A. Sihvola and J. A. Kong, "Effective permittivity of dielectric mixtures," *In Proceeding of IEEE on Trans. Geoscience and Remote Sensing* (IEEE, 1988), pp. 420–429.
23. V. Janicki, J. Sancho-Parramon, and H. Zorc, "Refractive index profile modeling of dielectric inhomogeneous coatings using effective medium theories," Thin Solid Films **516**(10), 3368–3373 (2008).
24. M. Skorobogatiy, *Nanostructured and Subwavelength Waveguide: fundamentals and applications* (Wiley, 2012).
25. C. Tuck, Choy, *Effective Medium Theory: Principles and Applications* (Oxford University Press, 1999).
26. S. Kedenburg, M. Vieweg, T. Gissibl, and H. Giessen, "Linear refractive index and absorption measurements of nonlinear optical liquids in the visible and near-infrared spectral region," Opt. Mater. Express **2**(11), 1588–1611 (2012).
27. G. A. Niklasson, C. G. Granqvist, and O. Hunderi, "Effective medium models for the optical properties of inhomogeneous materials," Appl. Opt. **20**(1), 26–30 (1981).
28. R. Röttgers, D. McKee, and C. Utschig, "Temperature and salinity correction coefficients for light absorption by water in the visible to infrared spectral region," Opt. Express **22**(21), 25093–25108 (2014).
29. W. S. Pegau, D. Gray, and J. R. Zaneveld, "Absorption and attenuation of visible and near-infrared light in water: dependence on temperature and salinity," Appl. Opt. **36**(24), 6035–6046 (1997).
30. J. M. Sullivan, M. S. Twardowski, J. R. V. Zaneveld, C. M. Moore, A. H. Barnard, P. L. Donaghay, and B. Rhoades, "Hyperspectral temperature and salt dependencies of absorption by water and heavy water in the 400-750 nm spectral range," Appl. Opt. **45**(21), 5294–5309 (2006).
31. L. Rindorf and O. Bang, "Highly sensitive refractometer with a photonic-crystal-fiber long-period grating," Opt. Lett. **33**(6), 563–565 (2008).
32. T. Wieduwilt, J. Dellith, F. Talkenberg, H. Bartelt, and M. A. Schmidt, "Reflectivity enhanced refractive index sensor based on a fiber-integrated Fabry-Perot microresonator," Opt. Express **22**(21), 25333–25346 (2014).
33. K. J. Lee, X. Liu, N. Vuillemin, R. Lwin, S. G. Leon-Saval, A. Argyros, and B. T. Kuhlmey, "Refractive index sensor based on a polymer fiber directional coupler for low index sensing," Opt. Express **22**(14), 17497–17507 (2014).
34. T. K. Yadav, R. Narayanaswamy, M. H. Abu Bakar, Y. M. Kamil, and M. A. Mahdi, "Single mode tapered fiber-optic interferometer based refractive index sensor and its application to protein sensing," Opt. Express **22**(19), 22802–22807 (2014).

1. Introduction

Refractive index (RI) values of materials are related to their composition. Measurement of analyte refractive index is important in numerous scientific and industry applications, such as bio-chemical sensing, material purity determination, concentration prediction, physical/chemical process monitoring [1–4]. Particularly, on-line monitoring of the solution concentrations, including heat transfer fluids, coolant, or other dilutions, is of significant importance in many industrial processes [5]. Liquid-core optical fibers is a very promising platform for refractive index sensing, as they inherently integrate optical detection with microfluidics, thus allowing for continuous on-line monitoring of liquid samples in a contained, highly-integrated manner.

Up to date, a wide range of liquid-core optical fiber sensors has been developed for RI measurement. For example, several sensors based on liquid-core fibers with total internal reflection (TIR) guidance have been proposed and demonstrated [6, 7]. These sensors typically operate using an amplitude-based sensing modality in which the transmission intensity of the liquid-core fiber is interrogated as a function of changes in the refractive index of a test analyte. While these sensors are advantageous due to their simple structures and sensing principle, the difficulty in finding suitable cladding material with refractive index lower than those of aqueous solutions (n~1.33) limits TIR liquid-core sensors for industrial applications.

Using sensors based on hollow-core (HC) photonic crystal fibers (PCFs) constitutes an alternative to the fibers with TIR guidance [8–10]. A defining feature of the PCFs is the

#237316 Received 23 Jun 2015; revised 17 Aug 2015; accepted 20 Aug 2015; published 24 Aug 2015

presence of micron-sized air holes running along its entire length, which permits accommodation of the biological and chemical samples in gaseous or liquid forms inside of the air holes in the immediate vicinity of the fiber core [13]. Photonic bandgap fibers (PBGFs), a subset of PCFs, are frequently used to build RI sensors. PBGFs sensors usually operate on a spectral-based detection modality. Variation in the real part of the analyte refractive index modifies the bandgap guidance of a fiber, leading to spectral shifts in the fiber transmission spectrum. The spectral shifts can be used to extract changes in the refractive index of a test analyte. In [11], the authors experimentally demonstrated highly sensitive liquid core RI sensors based on commercial HC-PBGFs that feature hollow core surrounded by porous periodic cladding. A sensitivity of ~5000 nm/RIU was reported. However, fabrication of HC-PBGFs used by the authors requires sophisticated drawing technique, and the fiber is expensive (thousands of dollars per meter). Moreover, these sensors require a relative long response time for filling test analytes into the micron-sized holes of the PBGFs [~10 min for 20cm-long PBGFs].

Hollow-core photonic bandgap Bragg fibers (or simply hollow-core Bragg fibers), which are a subset of PBGFs, could also be used for sensing of refractive index of a liquid analyte. In their cross section, a hollow core is surrounded by a periodic sequence of micron-sized layers of different materials in the cladding. Due to the relatively large core of Bragg fibers, the response time could be shortened to ~1s. In [12], K. J. Rowland et al reported a HC high-refractive-index-contrast Bragg fiber sensor with the sensitivity ~330nm/RIU. More recently, our group has reported several HC low-RI-contrast Bragg fiber sensors [13–15]. We showed that such Bragg fiber sensors offer superior performance in detection of changes in real part of the refractive index of a liquid analyte by monitoring the spectra shift of the transmission spectrum. The sensitivity of our sensor, compared to that of the sensor reported in [12], is considerably improved (~1400nm/RIU). In fact, we have argued in [14,16], that low-RI-contrast Bragg fibers are most suitable for liquid-core sensors, while high-RI-contrast Bragg fibers are most suitable for gas-core sensors.

In this paper, we explore the capability of the hollow core Bragg fibers to simultaneously monitor the real and imaginary parts of the analyte refractive index. We then apply our fiber sensor to monitor the concentrations of various commercial cooling oils. The sensing strategy relies on a two-channel sensing modality that simultaneous interrogates the bandgap center position of the Bragg fiber as well as the fiber transmission amplitude at the bandgap center (the point of fiber lowest propagation loss). Both measurands are highly sensitive to the complex reflective index of the analyte filling the fiber core, thus enabling efficient determination and cross-correlation with the concentration of cooling oils. The main advantage of the two-channel sensor compared to a single channel sensor is that, in principle, the measurement error can be significant improved if the two channels are independent and they offer comparable detection errors.

The fiber sensor is first calibrated using NaCl solutions of different concentrations. Measuring the spectral shift of the fiber bandgap, sensitivities to changes in the real part of the core refractive index are found to be ~1460nm/RIU, which translates into 2.6nm/w% sensitivity to changes in NaCl concentration. Additionally, using changes in the mid-bandgap transmission amplitude of the fiber sensor, sensitivities of 3.55dB/w% for NaCl solutions are demonstrated. We then apply this fiber sensor for monitoring the concentrations of various cooling oils including heat transfer fluid and sawing fluid. By using spectral modality and effective medium theory, we determine the concentrations of the two commercial fluids from the measured refractive indices with accuracy of ~0.57% for both low- and high-loss oils. Moreover, we also demonstrate that using an amplitude-based detection modality allows determination of the oil concentration with accuracy of ~1.64% for low-loss oils and ~2.81% for the high-loss oils. The presented fiber sensor can be used for on-line monitoring of concentration of many industrial fluids such as heat transfer fluids, sawing fluids, and other industrial dilutions with sub-1%v accuracy.

#237316 Received 23 Jun 2015; revised 17 Aug 2015; accepted 20 Aug 2015; published 24 Aug 2015

2. Operation principle of the liquid-core Bragg fiber sensors

2.1 Sensing mechanism for detection of the real part of an analyte refractive index

The Bragg fiber used in our sensor features a large hollow core (diameter ~700μm) surrounded by periodic sequence of high and low refractive index layers, namely polystyrene (PS)/poly-methacrylate (PMMA) Bragg reflector with layer refractive indices of 1.58 and 1.49 at 589nm, respectively. The cross section of the Bragg fiber sensor is shown in Fig. 1. The thickness of each PMMA/PS multi-layer is approximately 310nm.

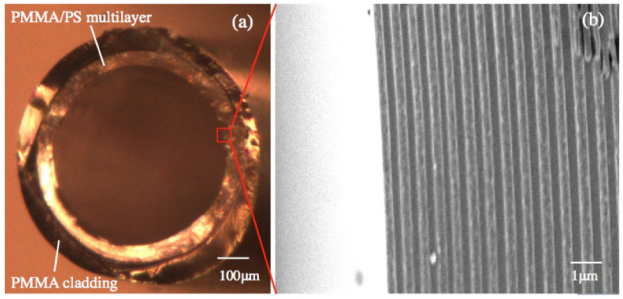

Fig. 1. (a) Cross section of the fiber sensor under microscope. (b) Cross section of the Bragg reflector taken by a scanning electron microscope (SEM), which features alternating polystyrene (PS) /poly-methacrylate (PMMA) layers, with thickness of approximately 310nm.

Bragg fibers confine light in their hollow cores by photonic bandgap effect. When broadband light is launched into the analyte-filled core of a Bragg fiber, only the light with frequencies within the fiber bandgap of Bragg reflector will be confined and guided in the fiber core, while the light with frequencies outside of the bandgap will be irradiated out in the first several centimeters of the fiber. From the basic theory [16,17] of the Bragg fibers, the resonant center wavelength λ_g, of the fiber fundamental bandgap can be calculated as:

$$\frac{\lambda_g}{2} = d_l\sqrt{\varepsilon_l^r - \varepsilon_c^r} + d_h\sqrt{\varepsilon_h^r - \varepsilon_c^r} \qquad (1)$$

where, d_l and d_h are the thicknesses of the low- and high- refractive index layers in the Bragg reflector, ε_l^r, ε_h^r are the real parts of the corresponding dielectric constants, while ε_c^r is the real part of the dielectric constant of the core material. Equation (1) is valid based on the assumption that the real part of any dielectric constant is much larger than its imaginary part. From Eq. (1), it follows that variation in the refractive index of the fiber core would modify spectral position of the Bragg fiber bandgap. In fact, one observes shift of the fiber transmission spectrum towards shorter wavelengths for larger values of the core dielectric constant. Therefore, changes in the real part of the refractive index of a test analyte filling the fiber core could be inferred from the displacement of the transmission spectrum, which constitutes the spectral-based sensing principle of a Bragg fiber sensor.

2.2 Sensing mechanism for detection of the concentration of additives in a liquid analyte

In many practical applications that involve mixtures of fluids, one is not so much interested in the refractive index of a mixture, but rather in the relative concentrations of the constituent fluids. In what follows, we consider a particular problem of monitoring concentration of cooling oils in aqueous mixtures (suspensions). In this case, a small amount of cooling oil together with surfactants is added into water to form a suspension. In such suspensions, spherical oil particles are deeply sub-wavelength. As a result, such suspensions appear clear and without any obvious phase separation, as shown in Fig. 2(a). At the same time, many oils

#237316 Received 23 Jun 2015; revised 17 Aug 2015; accepted 20 Aug 2015; published 24 Aug 2015

are colored emulsion and have significant frequency dependent absorption as shown in Fig. 2(b). In this section, we first show that the oil concentration could be inferred by using the spectral modality for the detection of the mixture refractive index and effective medium theory for relating the oil concentration to the mixture refractive index. We then demonstrate an amplitude-based detection modality of the Bragg fiber sensor for determining the oil concentration in a suspension by analyzing the transmission amplitude of an analyte-filled Bragg fiber at the bandgap center position.

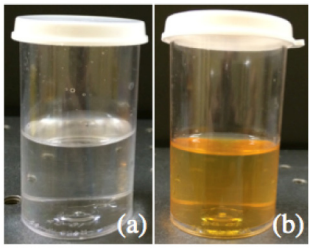

Fig. 2. (a) Low-loss cooling oil (heat transfer fluid), (b) High-loss cooling oil (sawing fluid).

2.2.1 Oil concentration detection using spectral modality and effective medium theory

Effective medium theory relates macroscopic properties of a mixture with its composition, and it has been widely used for modeling of various optical, electrical and thermal properties of mixtures [20–25]. According to effective medium theory, the effective dielectric constant of a mixture can be written as a function of the dielectric constant and the corresponding concentrations of its sub-components. For suspensions featuring small-to-medium concentrations (0-30%) of oil droplets in water, we could use Bruggeman (BG) formulation [25,27] to describe the dependence of the complex dielectric constant of suspension on oil concentration:

$$c \cdot \frac{\varepsilon_o - \varepsilon_{eff}}{\varepsilon_o + 2 \cdot \varepsilon_{eff}} + (1-c) \cdot \frac{\varepsilon_w - \varepsilon_{eff}}{\varepsilon_w + 2 \cdot \varepsilon_{eff}} = 0 \qquad (2)$$

Where ε_{eff} is the complex effective dielectric constant of the oil suspension in water, ε_o and ε_w are the complex dielectric constants of the pure bulk oil and water, respectively, c is the volume concentration of oil. If the bulk refractive indices of water and oil are known, using Eq. (2) one can calculate the concentration of oil in a suspension from the effective refractive index of a suspension. In turn, the effective refractive index of a suspension can be measured by using spectral modality of the Bragg fiber sensor, as discussed in Section 2.1.

2.2.2 Oil concentration detection using amplitude modality

When the Bragg fiber is filled with oil suspensions, the propagation loss of the fiber can be considered approximately as the sum of the fiber radiation losses and the absorption loss of the fiber core material.

The radiation loss is a direct consequence of the leaky-mode guidance in a core with refractive index smaller than that of the cladding. The radiation loss of Bragg fibers is frequency dependent. Consider, for example, a Bragg fiber with a certain number of bilayers in its Bragg reflector and a large diameter of a fiber core (much larger than the wavelength of light). According to Eq. 4.47 in [18], at the wavelength corresponding to the bandgap center, the radiation loss coefficient of the fundamental core-guided mode α_{rad} can be written as:

$$\alpha_{rad} = \Re(\mathrm{n}_c^r, \mathrm{n}_h^r, \mathrm{n}_l^r, \mathrm{d}_c, \mathrm{d}_h, \mathrm{d}_l) \qquad (3)$$

#237316 Received 23 Jun 2015; revised 17 Aug 2015; accepted 20 Aug 2015; published 24 Aug 2015

where, $\Re$ is a function dependent on the real part of the refractive index of the fiber core, as well as the geometry parameter and refractive indices of the low- and high- reflective index layers in a Bragg reflector. Note that when the concentration of a coolant increases, the refractive index of the coolant solution also increases. Consequently, the core refractive index of the liquid-filled Bragg fiber becomes closer to that of the fiber cladding. In the limit when the core refractive index becomes higher than that of the fiber cladding, no radiation losses will occur as the guidance regime will be total internal reflection rather than bandgap guiding. Therefore, the fiber radiation loss would decrease with an increase of the core refractive index, in other words with an increase in coolant concentration.

Absorption of the fiber core material also affects the fiber propagation loss. Consider, for example, filling the Bragg fiber with an analyte, which is a cooling oil diluted in water at concentration c. The effective absorption coefficient of such mixture, α_{eff} can be written as:

$$\alpha_{eff} = \Phi_o(\mathrm{c}) \cdot \alpha_o + \Phi_w(\mathrm{c}) \cdot \alpha_w \tag{4}$$

where, α_o and α_w are the material absorption coefficients of the pure cooling oil and water, respectively. The detailed expressions for $\Phi_o(c)$ and $\Phi_w(c)$ are presented in the appendix section.

With the fiber radiation loss and the fiber core absorption given by Eq. (3) and Eq. (4), we now can write the transmission of an analyte-filled Bragg fiber at the bandgap center as:

$$T(\lambda) = I/I_0 = e^{-(\alpha_{rad} + \alpha_{eff}) \cdot L} = e^{-[\Re + \Gamma \cdot (\Phi_o(c) \cdot \alpha_o + \Phi_w(c) \cdot \alpha_w)] \cdot \mathrm{L}} \tag{5}$$

where L is the length of the Bragg fiber, I and I_0 are the output and input intensities of light related to the fiber sensor. Γ is the confinement factor, which is a measure of the overlap between the optical mode and the fiber-core material. For a large-core Bragg fiber in our sensor, the optical mode can be considered completely confined in the core region, and Γ is very close to 1.

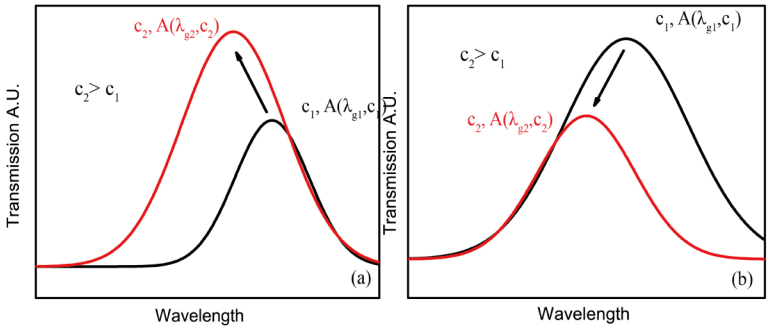

Fig. 3. Schematic of the two possible behavior of the Bragg fiber spectra when increasing the concentration of the cooling oil in the liquid-filled fiber core. (a) Low-absorption-loss cooling oil, (b) High-absorption-loss cooling oil.

When the Bragg fiber is filled with a solution of low-loss cooling oil, little or no additional absorption loss occurs when increasing concentration of the oil. At the same time, the fiber radiation loss decreases when increasing oil concentration due to increase in the mixture refractive index. Therefore, the total effect of the increase in the cooling oil concentration would be an enhancement in the Bragg fiber transmission, as shown in Fig. 3(a). However, when using high-loss cooling oils (those with a color tint), increasing in oil concentration leads to significant increase in the absorption loss of the liquid core. This in turn can be more pronounced than the decrease in the radiation loss, thus leading to suppression of transmission

#237316 Received 23 Jun 2015; revised 17 Aug 2015; accepted 20 Aug 2015; published 24 Aug 2015

through the liquid-core Bragg fiber, which results in higher attenuation at higher oil concentration, as shown in Fig. 3(b). In both cases, position of the bandgap center shifts to shorter wavelength with increase in oil concentration, according to Eq. (1).

In order to measure concentration of an unknown suspension using the amplitude modality, the Bragg fiber sensor should be first calibrated using a set of reference solutions (such as NaCl solutions) with known bulk absorption losses. During calibration, the transmission spectra of the Bragg fiber sensor filled with reference solutions are recorded. After calibration, the sensor can be used to measure the concentration of an oil suspension by comparing the transmission spectrum of the oil-filled Bragg fiber to the spectra of the fiber filled with the reference solutions. If the bandgap center position of the oil-filled Bragg fiber matches that of the Bragg fiber filled with a specific reference solution, the real parts of the refractive index of these two solutions would be identical as follows from Eq. (1). Moreover, we note that the radiation losses of the Bragg fiber filled with the oil suspension and the reference solution would be also identical as long as they have the same bandgap center wavelength, as seen from Eq. (3). Therefore, the difference in the transmission intensities of the fiber filled with oil suspension and reference solution sharing the same bandgap center wavelength are only attributed to the different absorptions of the liquids filling the fiber core. Comparing transmission of the Bragg fiber filled with oil suspension to transmission of the fiber filled with a reference solution (NaCl solution) for which the bandgap center wavelength λ_g is the same, we have:

$$\begin{aligned} T_{ref}(\lambda_g) &= e^{-(\Re+\Gamma\cdot\alpha_{ref})\cdot L} \\ T_{oil}(\lambda_g) &= e^{-[\Re+\Gamma\cdot(\Phi_o(c)\cdot\alpha_o+\Phi_w(c)\cdot\alpha_w)]\cdot L} \\ \Phi_o(c)\cdot\alpha_o+\Phi_w(c)\cdot\alpha_w &= \alpha_{ref}+\frac{1}{\Gamma\cdot L}\cdot Im\left(\frac{T_{ref}(\lambda_g)}{T_{oil}(\lambda_g)}\right) \end{aligned} \tag{6}$$

where, $T_{ref}(\lambda_g)$ and $T_{oil}(\lambda_g)$ refer to the transmission of the Bragg fiber filled with the reference solution and the oil solution to be measured at the same bandgap center wavelength λ_g, α_{ref} is the absorption of the reference solution, c is the concentration of the test oil. Note that, α_{ref}, α_o and α_w at wavelength λ_g should be measured using for example cut-back method [26]. Based on Eq. (6), one could then calculate the concentration of an oil suspension by solving a non-linear equation.

3. Experimental setup and calibration of the Bragg fiber sensor

3.1 Experimental set-up

The experimental set-up is shown in Fig. 4. The fiber sensor is integrated into the set-up using two opto-fluidic blocks, which enable both optical coupling and flow of the target analytes. After pumping liquid analyte into the sensor, a beam from a broadband supercontinuum source is launched into one end of the fiber core using an objective. The transmitted spectrum is registered by a grating spectrometer. The experimental set-up is kept the same in the subsequent measurements to guarantee same coupling and environmental conditions.

#237316 Received 23 Jun 2015; revised 17 Aug 2015; accepted 20 Aug 2015; published 24 Aug 2015

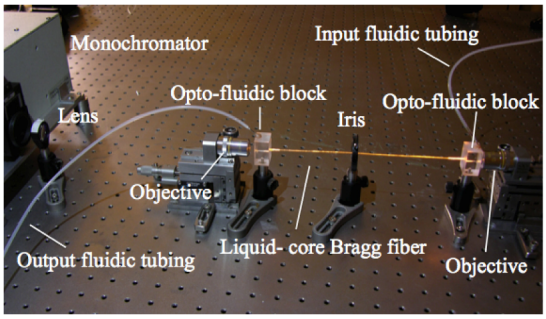

Fig. 4. Experimental set-up of the fiber sensor. The 24cm long Bragg fiber is integrated into the set-up using two opto-fluidic blocks. A broadband supercontinuum beam is launched into one end of the liquid-core Bragg fiber using an objective, and the output spectrum of the fiber sensor is registered by a grating monochromator.

3.2 Calibration of the Bragg fiber sensor with NaCl solutions

A calibration measurement of the Bragg fiber sensor is first carried out using a set of NaCl solutions with the weight concentration ranging from 0% to 10% with a 2% increment step. The RIs of NaCl solutions are obtained from [19]. As shown in Fig. 5(a), the experimental transmission spectra feature a blue shift as the RIs of the NaCl solutions filling the core increase with increased concentration of NaCl. This can be easily rationalized using Eq. (1) by noting that higher concentrations of NaCl in water lead to higher refractive indices of the resultant solutions. A spectral shift of around 26 nm is observed when the refractive index of the core material increases from 1.333 to 1.3505 (with corresponding concentration from 0%w to 10%w), as is shown in Fig. 5(b). The spectral sensitivity is thus found to be ~1460nm/RIU, which translates into 2.6nm/w% sensitivity to changes in the NaCl concentration. The demonstrated sensitivity is comparable with those of the recently reported fiber-based refractive index sensors [31–34].

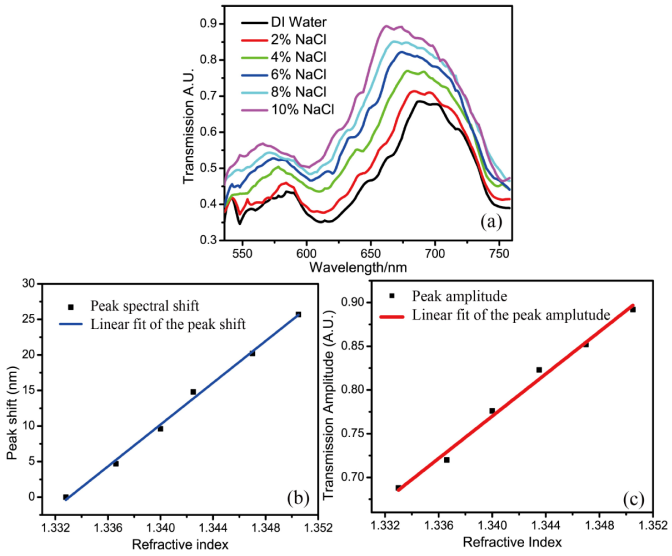

Fig. 5. (a) Experimental transmission spectra of the ~24cm long Bragg fiber filled with NaCl solutions. The weight concentrations (wt.%) and the corresponding RIs of the NaCl solutions are listed as following. DI water: 1.333, 2%: 1.3366, 4%: 1.3400, 6%: 1.3435, 8%: 1.3470, 10%: 1.3505. (b) Spectral shifts of the fiber maxima transmission peaks obtained from the experimental measurements and their linear fit. (c) Transmission amplitudes at the maxima transmission peaks obtained from the experimental measurements and their linear fit.

#237316 Received 23 Jun 2015; revised 17 Aug 2015; accepted 20 Aug 2015; published 24 Aug 2015

Moreover, the transmission amplitude increases with the increase of the refractive index of the fiber core. Figure 5(c) shows the transmission amplitude at the point of the fiber lowest propagation loss as a function of the refractive index of the fiber core. From the linear fit in Fig. 5(c), the amplitude sensitivity of the sensor is 301.7 dB/RIU, which translates into a sensitivity of 3.55dB/w% for NaCl solution. In the following sections, we will use the obtained calibration spectra and linearly fitted spectral and amplitude data presented in Fig. 5 in order to measure the refractive index and concentration of the unknown aqueous mixtures.

3.3 Measurements of the bulk absorption coefficients of pure oil, water and a solution (NaCl)

In order to profit from a two-channel modality for determination of the oil concentration, we have to perform both spectral Eq. (1) and amplitude Eq. (6) measurements. The latter requires knowledge of the bulk absorptions of oil, water and NaCl reference solutions. In this section, we present a cut-back technique to measure the required absorption coefficients.

According to a cut-back technique, losses of the two identically prepared material samples of different lengths have to be measured in order to determine the bulk absorption coefficient of the material. Then, the ratio of the transmitted intensities through the samples of different lengths (L_1, L_2) at wavelength λ is:

$$\frac{I_{liquid}(\mathrm{L}_1,\lambda)}{I_{empty}(\mathrm{L}_1,\lambda)} \Big/ \frac{I_{liquid}(\mathrm{L}_2,\lambda)}{I_{empty}(\mathrm{L}_2,\lambda)} = e^{\alpha_{abs}\cdot(\mathrm{L}_2-\mathrm{L}_1)} \tag{7}$$

where the transmitted intensity through the empty tube I_{empty} is used as a reference signal. Rewriting Eq. (7), one can calculate the absorption coefficient as:

$$\alpha_{abs}(\lambda) = \frac{In\left(\frac{I_{liquid}(\mathrm{L}_1,\lambda)}{I_{liquid}(\mathrm{L}_2,\lambda)} \cdot \frac{I_{empty}(\mathrm{L}_2,\lambda)}{I_{empty}(\mathrm{L}_1,\lambda)}\right)}{L_2 - L_1} \tag{8}$$

The experimental set-up for absorption measurement using a cut-back technique is illustrated in Fig. 6(a). We use three rectangular containers with different lengths (5cm, 10cm, and 15cm) in our measurements. From the transmission spectra for each tube length and the corresponding reference measurements, one can calculate the wavelength dependent absorption coefficient using Eq. (8). An average absorption coefficient is calculated from several possible combinations of the different sample lengths in Eq. (8).

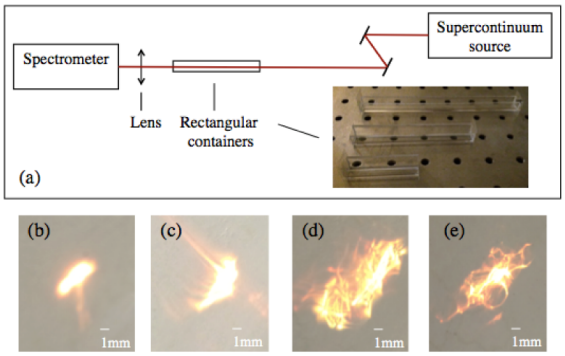

Fig. 6. (a) Experimental set-up for bulk absorption measurements using a cut-back technique, inset: containers of different length (5cm, 10cm, 15cm). (b) and (c) Optical beam output spot at the end-face of a container filled with the low-loss heat-transfer fluid. (d) and (e) Optical beam output spot at the end-face of a container filled with the high-loss sawing fluid. During measurements, the output spots at the end-face of the container are somewhat distorted and vary with time, the time intervals between (b) and (c), as well as (d) and (e) are both five minutes.

#237316 Received 23 Jun 2015; revised 17 Aug 2015; accepted 20 Aug 2015; published 24 Aug 2015

In Fig. 7(a), we plot the measured absorption coefficients of distilled water, and a set of NaCl solutions at concentration of 3%, 6%, and 9% (by weight) from 650nm to 700nm with interval of 2nm. We note that the experimental values of absorption coefficients measured using a cut-back method in this work are 1.5 to 1.8 times higher than the values reported in [28–30]. This is probably due to the effect of unequal coupling into the spectrometer when the containers are filled with solutions of different refractive indices.

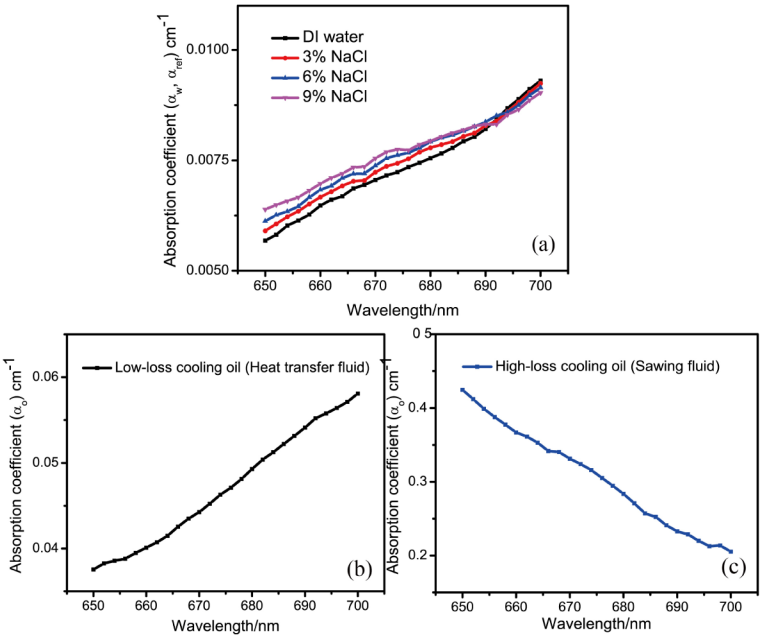

Fig. 7. (a) Absorption coefficients of distilled water and NaCl solutions at concentrations of 3%, 6%, and 9% (by weight) measured using a cut-back technique. (b) Absorption coefficients of the low-loss-absorption oil (heat-transfer fluid) measured using a cut-back technique and (c) Absorption coefficients of the high-absorption-loss oil (sawing fluid) measured using a cut-back technique

From Fig. 7(a), we can extract the salinity correction coefficient for water absorption. Thus, the absorption coefficient of NaCl solution at any concentration can be calculated [28]. In Figs. 7(b) and 7(c), we plot the absorption coefficients of the low-loss cooling oil (heat transfer fluid), and the high-loss cooling oil (sawing fluid). During the measurement, we notice that the optical beam output spots at the end-face of the container are somewhat distorted and vary with time, as it is shown in Figs. 6(b)-6(e). This is most probably due to certain microscopic movement and relaxation dynamics of the cooling oils.

4. Two-channel characterization of concentrations of the heat transfer fluids

After sensor calibrations described in Section 3, we use it to first measure the real part of the refractive index of the cooling oil suspension by employing spectral modality. We choose, as the first analyte, a commercial heat-transfer fluid (Dynalene PG, US, shown in Fig. 2(a)) at three different concentrations 5%, 10% and 15% (by volume). As shown in Fig. 8(a), the transmission spectrum has a blue-shift of 7.2nm, 17nm and 24.7nm, compared to the transmission spectrum of the Bragg fiber filled with water. Based on the linear fit of the refractive indices of the reference solutions presented in Fig. 5(b), we estimate the real part of the refractive indices of these heat-transfer fluids to be 1.3380, 1.3432, and 1.3492, respectively. These measured values show a good agreement with the reference data provided by the supplier as shown in Fig. 8(b).

#237316 Received 23 Jun 2015; revised 17 Aug 2015; accepted 20 Aug 2015; published 24 Aug 2015

We then reconstruct the concentrations of heat-transfer fluids with the algorithm based on the effective medium theory presented in Section 2.2.1. Substituting the refractive indices of the heat-transfer fluids in to Eq. (2), we calculate the concentrations of the corresponding analytes based on the BG model. In Fig. 8(c), we plot the experimental concentration and the concentration predicted by the BG model as a function of the refractive index. The reconstruction accuracy in determining the fluid concentration in this case is ~0.42%.

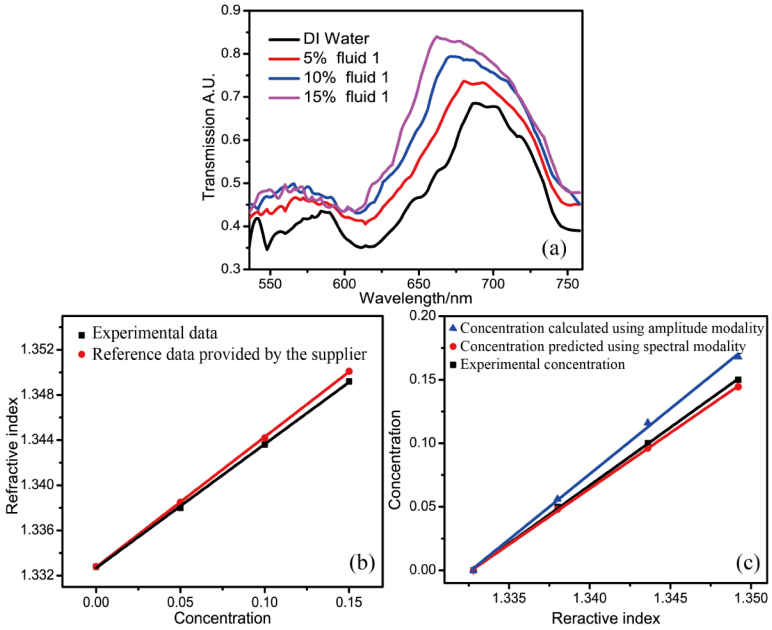

Fig. 8. (a) Experimental transmission spectra of the 24cm long Bragg fiber filled with heat-transfer fluid at different concentrations (by volume). (b) Comparison of the refractive indices measured in experiment and the reference data provided by the supplier. (c) Comparison of the experimental concentrations with the concentrations predicted using spectral measurement modality and the BG model, as well as concentrations calculated using amplitude-based detection modality.

We now analyze the transmission amplitudes of the Bragg fiber filled with the oil suspensions. From the previous experiment we have established that suspensions of heat-transfer fluid at concentrations of 5%, 10%, and 15% have the same refractive indices as that of NaCl solution at concentrations of 3%, 6.4%, and 9.5%, respectively. Note that the transmission amplitude of the Bragg fiber filled with NaCl solutions could be estimated based on the linear fit shown in Fig. 5(c). The absorption coefficients of the pure heat-transfer fluid and the reference NaCl solutions have been measured in Section 3.3. Using Eq. (6), we can now calculate concentrations using amplitude modality. The data is presented in Fig. 8(c). The accuracy in determination of oil concentration is found to be ~1.64%. We note that the error is mainly due to the following two reasons. First, in our theoretical calculation the scattering loss is assumed to be negligible. However, in practice, small particles (such as dust particles) or air bubbles may be introduced during fluid pumping, which leads to errors in the measurement of transmission amplitude. Second, there is a certain error that comes from the cut-back measurement of absorption coefficients of the cooling oil. As we illustrated in Section 3.3, the optical beam output spot at the end-face of the container vary with time when measuring the absorption coefficient due to certain microscopic movement and relaxation dynamics of the cooling oil.

#237316 Received 23 Jun 2015; revised 17 Aug 2015; accepted 20 Aug 2015; published 24 Aug 2015

5. Two-channel characterization of concentrations of sawing fluids

Many commercial oils are colored emulsions, which have frequency dependent absorption. In this experiment, we choose as a test analyte commercial sawing fluid (Lenox, US, as shown in Fig. 2(b)) that has a yellow tint upon visual examination. The transmission spectra of the fiber sensor are shown in Fig. 9(a). Despite the strong absorption loss, we see that the spectral features (transmission peaks) in the transmission spectrum remain well pronounced. Using the linear fit in Fig. 5(b), the refractive indices of the emulsions are estimated to be 1.3332, 1.3342, 1.3351, 1.3375, when volume concentrations of sawing fluid are 1%, 3%, 5% and 10%, respectively. These experimentally measured values of the refractive index are in good agreement with the calibration data provided by the fluid suppliers as shown in Fig. 9(b).

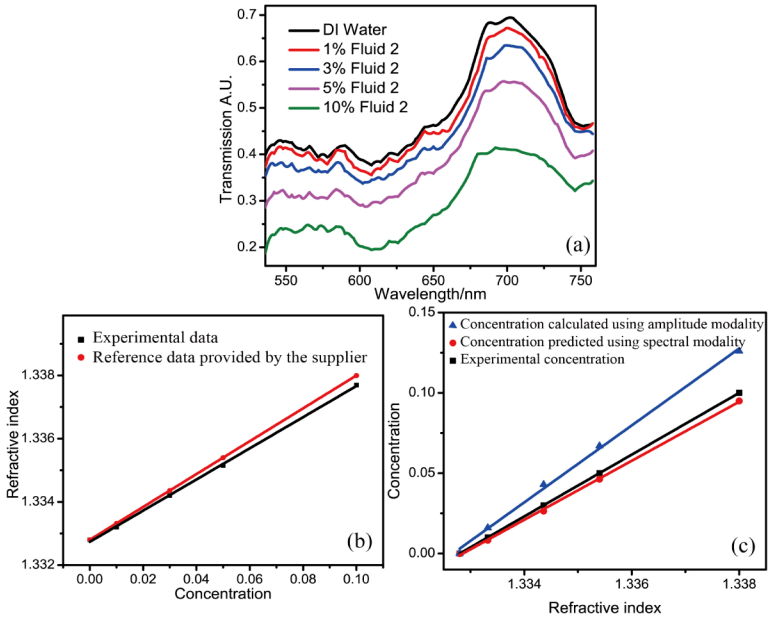

Fig. 9. (a) Experimental transmission spectra of the 24cm long Bragg fiber filled with sawing fluid at different concentrations (by volume). (b) Comparison of the refractive indices measured in experiment and the reference data provided by the supplier. (c) Comparison of the experimental concentrations with the concentrations predicted by spectral modality and the BG model, as well as concentrations calculated using amplitude-based detection modality.

Using effective medium theory, we can then extract sawing fluid concentration from the measured values of the refractive index by using BG model. Figure 9(c) shows the experimental concentrations and concentrations predicted by the BG model as a function of the refractive index. The reconstructed accuracy in this case is ~0.57%.

We then apply the amplitude modality to determine the concentrations of sawing fluids using the same methodology as presented in Section 4. In Fig. 9(c), we plot the calculated concentrations by amplitude modality and the experimental concentrations as a function of the refractive index. The accuracy in this case is found to be ~2.81%, which is worse than that for a low-loss heat-transfer fluid. The primary reason is due to low precision in the measured value of the bulk absorption loss of sawing fluid when using a cut-back method.

6. Discussion

In this paper, we proposed two detection modalities for monitoring concentrations of commercial cooling oils by analyzing the bandgap center position and transmission amplitude at the mid-bandgap of the analyte-filled Bragg fiber. First, when using spectral detection

#237316 Received 23 Jun 2015; revised 17 Aug 2015; accepted 20 Aug 2015; published 24 Aug 2015

modality, oil concentration could be inferred from the suspension refractive index by using Bruggeman effective medium theory. Alternatively, when using amplitude detection modality, oil concentration could be found by fitting changes in the suspension absorption losses and comparing them to losses of a reference solution.

In principle, using multiple-channel detection modalities for measuring an experimental value could enhance the detection accuracy, since the measurement uncertainty could become smaller by a factor of $1/\sqrt{N}$, when N detection channels with comparable detection errors are used. However, because of unstable optical output of the cooling oils when measuring the absorption coefficients using a cut-back technique, the accuracy of amplitude detection modality is much worse than that of spectral modality, therefore, the accuracy of our sensor for monitoring the oil concentration cannot be enhanced by using the two detection modalities. In our future work, we will have to balance the accuracies of the two sensing channels in order to enhance the overall accuracy of the two-channel Bragg fiber sensor.

7. Conclusion

In summary, we demonstrate simultaneous monitoring of the real and imaginary parts of the liquid analyte refractive index by using a hollow-core Bragg fiber, and we apply this fiber sensor to monitor concentrations of various commercial liquids by monitoring of the fiber bandgap center wavelength, as well as the fiber transmission amplitude at the point of fiber lowest propagation loss (bandgap center). The fiber sensor is first calibrated using NaCl solutions of different concentrations. By measuring spectral shift of the fiber bandgap, the sensitivities to changes in the real part of the core refractive index are found to be 1460nm/RIU, which translates into a sensitivity of 2.6nm/w% to changes in the concentration of a NaCl solution. Additionally, using changes of transmission amplitude at the point of fiber lowest propagation loss of the Bragg fiber, a concentration sensitivity of 3.55dB/w% for NaCl solutions is obtained. By using spectral modality and effective medium theory, we determine the concentrations of the two commercial fluids from the measured refractive indices with accuracy of ~0.57% for both low- and high-loss oils. Moreover, we also demonstrate that using an amplitude-based detection modality allows determination of the oil concentration with accuracy of ~1.64% for low-loss oils and ~2.81% for the high-loss oils. The proposed Bragg fiber sensor has the advantages such as simple structure, fast response, and low cost. One practical application of the proposed sensor is precision monitoring of the cooling oil concentration in cooling solutions and sawing liquids, where real time monitoring of oil concentration with sub-1%v accuracy is desired.

Appendix:

In the appendix, we provide derivation of the expression for the effective absorption coefficient of a two-component mixture suspension (cooling oil diluted in water at concentration c) using effective medium theory.

The effective absorption coefficient of a suspension is related to the imaginary part of its effective dielectric constant. The dependence of the complex dielectric constant of a suspension on the oil concentration can be described using Bruggeman (BG) model for suspensions featuring small-to-medium concentrations (0-30%) of oil droplets in water. To extract the relation between the imaginary part of the effective dielectric constant and the oil concentration, we write the BG formulation Eq. (2) using complex values of the dielectric constants:

$$c\cdot\frac{\varepsilon_o^r+i\cdot\varepsilon_o^i-\left(\varepsilon_{eff}^r+i\cdot\varepsilon_{eff}^i\right)}{\varepsilon_o^r+i\cdot\varepsilon_o^i+\left(\varepsilon_{eff}^r+2i\cdot\varepsilon_{eff}^i\right)}=(c-1)\cdot\frac{\varepsilon_w^r+i\cdot\varepsilon_w^i-\left(\varepsilon_{eff}^r+i\cdot\varepsilon_{eff}^i\right)}{\varepsilon_w^r+i\cdot\varepsilon_w^i+\left(\varepsilon_{eff}^r+2i\cdot\varepsilon_{eff}^i\right)} \qquad (9)$$

#237316 Received 23 Jun 2015; revised 17 Aug 2015; accepted 20 Aug 2015; published 24 Aug 2015

where ε_{eff} is the complex effective dielectric constant of the oil suspension in water, ε_o and ε_w are the complex dielectric constants of the pure bulk oil and water, respectively. Manuscripts r and i refer to the real and imaginary parts of the dielectric constants.

Assuming that the imaginary part of any dielectric constant is much smaller than the real part of any dielectric constant for the analytes involved in this paper, the imaginary part of the dielectric constant of the effective medium in Eq. (9) can be considered as a small correction to its real part. We then expand Eq. (9), and only retain the first-order terms, thus obtaining:

$$\varepsilon_{eff}^{i} = \varepsilon_{o}^{i} \cdot \frac{\varepsilon_{eff}^{r} - 3c \cdot \varepsilon_{eff}^{r} - \varepsilon_{w}^{r}}{3c\varepsilon_{o}^{r} - \varepsilon_{o}^{r} + 2\varepsilon_{w}^{r} - 3c\varepsilon_{w}^{r} - 4\varepsilon_{eff}^{r}} + \varepsilon_{w}^{i} \cdot \frac{-\varepsilon_{o}^{r} + 3c\varepsilon_{eff}^{r} - 2\varepsilon_{eff}^{r}}{3c\varepsilon_{o}^{r} - \varepsilon_{o}^{r} + 2\varepsilon_{w}^{r} - 3c\varepsilon_{w}^{r} - 4\varepsilon_{eff}^{r}} \quad (10)$$

Then, using $\varepsilon^{i} = 2n^{r} \cdot n^{i} = 2n^{r} \cdot \frac{\lambda \cdot \alpha_{abs}}{4\pi}$ into Eq. (10), we get:

$$\alpha_{eff} = \alpha_{o} \cdot \frac{n_{o}^{r}}{n_{eff}^{r}} \cdot \frac{\varepsilon_{eff}^{r} - 3c \cdot \varepsilon_{eff}^{r} - \varepsilon_{w}^{r}}{3c\varepsilon_{o}^{r} - \varepsilon_{o}^{r} + 2\varepsilon_{w}^{r} - 3c\varepsilon_{w}^{r} - 4\varepsilon_{eff}^{r}} + \alpha_{w} \cdot \frac{n_{w}^{r}}{n_{eff}^{r}} \cdot \frac{-\varepsilon_{o}^{r} + 3c \cdot \varepsilon_{eff}^{r} - 2\varepsilon_{eff}^{r}}{3c\varepsilon_{o}^{r} - \varepsilon_{o}^{r} + 2\varepsilon_{w}^{r} - 3c\varepsilon_{w}^{r} - 4\varepsilon_{eff}^{r}} \quad (11)$$

Based on Eq. (11), we then write α_{eff} as:

$$\begin{aligned} \alpha_{eff} &= \Phi_{o}(\mathrm{c}) \cdot \alpha_{o} + \Phi_{w}(\mathrm{c}) \cdot \alpha_{w} \\ \Phi_{o}(\mathrm{c}) &= \frac{n_{o}^{r}}{n_{eff}^{r}} \cdot \frac{\varepsilon_{eff}^{r} - 3c \cdot \varepsilon_{eff}^{r} - \varepsilon_{w}^{r}}{3c\varepsilon_{o}^{r} - \varepsilon_{o}^{r} + 2\varepsilon_{w}^{r} - 3c\varepsilon_{w}^{r} - 4\varepsilon_{eff}^{r}} \\ \Phi_{w}(\mathrm{c}) &= \frac{n_{w}^{r}}{n_{eff}^{r}} \cdot \frac{-\varepsilon_{o}^{r} + 3c \cdot \varepsilon_{eff}^{r} - 2\varepsilon_{eff}^{r}}{3c\varepsilon_{o}^{r} - \varepsilon_{o}^{r} + 2\varepsilon_{w}^{r} - 3c\varepsilon_{w}^{r} - 4\varepsilon_{eff}^{r}} \end{aligned} \quad (12)$$

#237316 Received 23 Jun 2015; revised 17 Aug 2015; accepted 20 Aug 2015; published 24 Aug 2015